Proc. Indian Acad. Sci. (*Chem. Sci.*), Vol. 113, No. 4, August 2001, pp 307–324
© Indian Academy of Sciences

An investigation of the photo-reactive and unreactive polymorphs of *o*-ethoxy cinnamic acid and of its photodimer

R SRINIVASA GOPALAN and G U KULKARNI*
Chemistry and Physics of Materials Unit, Jawaharlal Nehru Centre for Advanced Scientific Research, Jakkur PO, Bangalore 560 064, India
e-mail: kulkarni@jncasr.ac.in

MS received 29 November 2000

Abstract. Detailed X-ray crystallographic investigation of the reactive *a*- and the unreactive *g*-polymorphs of *o*-ethoxy cinnamic acid has been carried out along with that of the photodimer, *a*-truxillic acid. The molecule is quite planar in the *a*-form, but in the *g*-form, the side groups deviate significantly from the plane of the benzene ring. The carboxylic groups form normal cyclic hydrogen bonds in the *a*-form and near-symmetric hydrogen bonds in the *g*-form. The infrared spectrum of the *a*-form shows the characteristic features of the cyclic dimer, but that of the *g*-form is entirely different, marked by the absence of the O–H stretching band in the 3000 cm^{-1} region. Charge density analysis throws some light on the structure and reactivity of the molecule in the two forms. The near-symmetric hydrogen bond in the *g*-form is ionic and appears to restrict conjugation by way of distorting the molecule. This unusual feature keeps the cinnamoyl double bonds away from each other, rendering it photochemically unreactive. In the *a*-form, however, the double bonds have a closer approach. The cyclobutyl ring of the photodimer consists of weak single bonds, with the new pair being slightly longer.

Keywords. Photoreactivity; polymorphism; ethoxy cinnamic acid; electronic charge density; X-ray structure.

1. Introduction

Photochemical dimerization in cinnamic acid and its derivatives, first investigated by Cohen *et al*[1], is a classic in organic solid state chemistry. They established the general requisites for this (2+2) cycloaddition reaction to occur in the solid state. An important requirement for the reaction is the near parallel orientation of the reactive double bonds and a relatively short distance (3·7–4·2 Å) between them, the approach involving small displacive or angular motions. The cinnamic acids generally exist in polymorphic forms. The reactive *a*- and *b*-forms undergo photochemical dimerization to yield the corresponding symmetry-related *a*-truxillic acid and the *b*-truxinic acid respectively. The *g*-form, where it exists, is photostable. Based on a single crystal–single crystal X-ray diffraction study of the photodimerization of the *a*-form of *trans*-cinnamic acid, Enkelmann *et al*[2] found that the double bonds of the incipient cyclobutane ring show large displacements, while the phenyl and the carboxylic groups remain essentially in

*For correspondence

place. It was our desire to carry out thorough crystallographic investigation of both the reactive and the unreactive forms of cinnamic acid, to see how the structural features relate to the reactivity. For this purpose, we have determined the structures of the *a*- and *g*-forms of *o*-ethoxy cinnamic acid as well as of the photodimer of the *a*-form. The present study shows how the intermolecular hydrogen bond is significantly different in the *a*- and the *g*-forms and that in the latter it is primarily responsible for rendering the molecule non-planar and photochemically unreactive.

Charge density analysis is useful in understanding intra- and intermolecular bonding as well as properties and reactivities of molecular crystals [3]. Ortmann *et al* [4] applied this method to study a photoreactive pyrone molecule in comparison with an isoelectronic photostable oxazinone. Madsen *et al* [5] have studied hydrogen bonds with very short O···O contacts. A charge density study of *p*-nitrophenol has established interesting differences between two polymorphs of this compound, one of which is photochemically active [6]. In this paper, we report charge-density analysis of the reactive *a*- and the unreactive *g*-forms of *o*-ethoxy cinnamic acid. We observe that the charge concentrations in various regions are more even in the *a*-form compared to those in the *g*-form. There are significant differences in the hydrogen bond regions as well.

2. Experimental

o-Ethoxy cinnamic acid was prepared by the Knoevenagel reaction of *o*-ethoxy benzaldehyde and malonic acid in pyridine containing traces of bipyridine [7]. The *a*-form was obtained by the slow evaporation of a concentrated solution in ethyl acetate while slow cooling of a solution in ethanol–water mixture gave the *g*-form. The process of cooling from 75°C to room temperature was carried out over a period of three days. Unlike *trans*-cinnamic acid [2], the *o*-ethoxy cinnamic acid does not favour single crystal–single crystal photodimerization. In order to obtain the photodimer, 2,2′-diethoxy *a*-truxillic acid (*trans*-2,4-*bis*(2-ethoxyphenyl)-*trans*-1,3-cyclobutane dicarboxylic acid), crystals of the *a*-form were irradiated at room temperature using a mercury vapour lamp. After about an hour, the resulting compound was cleaned with copious amounts of ether, when the unreacted parent material went into solution while the product remained insoluble. This process was carried out a few times in order to remove all traces of the parent compound. The photodimer was dissolved in hot glacial acetic acid and filtered before crystallizing it under slow evaporation.

High quality crystals of *a*- and *g*-forms of the *o*-ethoxy cinnamic acid and of the dimer were chosen after examination under an optical microscope. X-ray diffraction intensities were measured by *w* scans using a Siemens three-circle diffractometer attached to a CCD area detector and a graphite monochromator for the MoK*a* radiation (50 kV, 40 mA). The crystals were cooled to 130 K on the diffractometer using a stream of cold nitrogen gas from a vertical nozzle and this temperature was maintained throughout the data collection. The infrared spectra of the *a*- and the *g*-forms were recorded with a Brüker IFS 66 v/S infrared spectrometer.

Unit cell parameters and orientation matrix of the crystal were initially determined using ~ 60 reflections from 25 frames collected over a small *w* scan of 7·5° sliced at 0·3° interval. A hemisphere of reciprocal space was then collected in two shells using the SMART software [8] with 2*q* settings of the detector at 28° and

70°. Data reduction was performed using the SAINT program[8] and the orientation matrix along with the detector and the cell parameters were refined for every 40 frames on all the measured reflections. The various experimental details are listed in table 1. The crystal structure was first determined with the low-resolution data up to $\sin q/l = 0{\cdot}56$ Å^{-1}. The phase problem was solved by direct methods and the non-hydrogen atoms were refined anisotropically, by means of the full matrix least squares procedures using SHELXTL[9]. The H atom positions were found using the difference Fourier method and were adjusted to average neutron values[10] (C_{sp^3}–H,

Table 1. Crystal data and experimental details.

Crystal	*a*	*g*	*a*-dimer
Chemical formula	$C_{11}H_{12}O_3$	$C_{11}H_{12}O_3$	$C_{22}H_{24}O_6$
Formula weight (g)	192·21	192·21	384·41
Cell system	Triclinic	Monoclinic	Monoclinic
Space group	*P* –1	*C* 2/*c*	*P* $2_1/c$
a (Å)	6·69530(10)	16·9695(2)	8·333(4)
b (Å)	8·67300(10)	5·46140(10)	8·444(2)
c (Å)	9·98270(10)	23·0688(3)	13·975(4)
a (°)	72·0270(10)	90	90
b (°)	71·1900(10)	110·8560(10)	106·64(3)
g (°)	67·7830(10)	90	90
V (cm^3)	496·326(11)	1997·87(5)	942·0(6)
Z	2	8	2
F_{000}	204	816	408
r (Mg m^{-3})	1·286	1·278	1·355
Radiation type	Mo K*a*		
Wave length (Å)	0·71073		
No. of reflections for cell parameters	60	60	60
m (mm^{-1})	0·093	0·093	0·10
Crystal form	Cuboidal	Needle	Cuboidal
Crystal size (mm)	0·3 × 0·2 × 0·2	0·3 × 0·15 × 0·15	0·15 × 0·1 × 0·1
Crystal color	Colourless	Colourless	Colourless
Data collection temperature	130(2) K	130(2) K	130(2) K
Diffractometer	Siemens CCD		
Crystal-detector distance (cm)	5·0		
No. of measured reflections	7405	14190	9163
No. of independent reflections	6365	8371	4928
No. of observed reflections	4120	5079	3711
R_{int}	0·0205	0·0299	0·0535
q_{min} (°)	2·21	1·89	2·55
q_{max} (°)	49·48	49·60	49·49
Range of *h*, *k*, *l*	$-11 \le h \le 13$	$-36 \le h \le 36$	$-16 \le h \le 17$
	$-18 \le k \le 18$	$-10 \le k \le 10$	$-17 \le k \le 18$
	$-16 \le l \le 21$	$-49 \le l \le 27$	$-25 \le l \le 28$
After multipole refinement			
Weighting scheme	0·07160, 0·1721	0·0737, 0·4	0·0731, 2·7123
R1	0·0426	0·0557	0·0417
wR2	0·0467	0·0654	0·0677
S	0·9808	0·9622	0·9388
No. of variables	278	278	278
N_{ref}/N_v	14·3	18·3	13·3

1·06 Å; C_{sp^2}–H, 1·075 Å; O–H, 0·96 Å) except in the case of the hydroxyl hydrogen of the *g*-form, which was held at the position obtained from the structure determination (for details, see §3). Rigid bond tests of the various bonds were also carried out using TLS routine of the THMA14c program [11]. In all the structures studied, the bonds closely satisfied the Hirshfeld criterion [12]. The largest librational components obtained from the TLS analysis were 4·02, 4·03 and 5·6 degree^2 for the *a*-, *g*- and the dimer structures respectively.

Charge density analysis was carried out based on multipole expansion of the electron density centred at the nucleus of the atom [13]. Accordingly, the aspherical atomic density can be described in terms of spherical harmonics,

$$r_{\text{atom}}(r) = r_{\text{core}}(r) + r_{\text{valence}}(r) + r_{\text{def}}(r).$$

Thus for each atom,

$$r_{\text{atom}}(r) = r_{\text{core}}(r) + P_v k^3 r_{\text{valence}}(kr) + \sum_{l=0} k'^3 R_l(k'zr) \sum_{m=0} \sum_{p=\pm 1} P_{\text{lmp}} Y_{\text{lmp}}(q, j),$$

with the origin at the atomic nucleus. The population coefficients, P_{lmp} are to be refined along with the k and k' parameters. The kappa parameters control the radial dependence of the spherical and deformation valence densities. The analysis was carried out in several steps.

High-order refinement of the data was first performed using reflections with $\sin q/l \geq 0{\cdot}6$ Å^{-1} and $Fo \geq 4s$. All the hydrogens were held constant throughout the refinement along with their isotropic temperature factors. Multipolar refinement for the charge density analysis was carried out using the XDLSM routine of the XD package [14] and the details are given in table 1. The atomic coordinates and the thermal parameters obtained from the high-order refinement were used as input to XD refinement. Oxygen and carbon atoms were refined up to octapole moments while hydrogens were restricted to dipole. Charge neutrality constraint was applied to the molecule during the refinement. The multipolar refinement strategy was the following: (a) Scale factor; (b) P_v; (c) P_{lm} (steps b and c until convergence); (d) k; (e) steps b and c till convergence; (f) k'; (g) steps b and c till convergence; (h) positional and thermal parameters of all non-hydrogen atoms, and finally (i) P_v and P_{lm} together. Static deformation density was obtained as a difference between the total density and the spherical density without the thermal smearing. Deformation density maps were plotted using the XDGRAPH routine. Residual maps obtained as the difference between the calculated and experimental densities were featureless, the magnitude of the random peaks being less than 0·12 eÅ^{-3}. The XDPROP routine was used to calculate the total electron density, $r(r)$, the Laplacian, $\nabla^2 r$, and the ellipticity, e, at the bond critical points (CPs). The value of r_{CP} is a measure of bond strength for a given pair of covalently bonded atoms [15] while the Laplacian signifies the extent of depletion or concentration of bonding density. Ellipticity measures the extent of conjugation. Other bond properties such as the polarization (Δ%) of the CP from the midpoint of the internuclear vector and its vertical displacement, d, denoting the polarity and the bent nature of a bond respectively, were also calculated. All the intramolecular CPs were of (3, –1) type [16] in $r(r)$ with negative Laplacians, characteristic of covalently bonded molecular systems [17]. Intermolecular

hydrogen contacts as determined by the PARST program [18] were of (3, –1) type with positive Laplacians, characteristic of closed shell interactions.

3. Results and discussion

We shall first discuss the molecular structures in the *a*- and the *g*-forms of *o*-ethoxy cinnamic acid. The *a*-polymorph exists in a centrosymmetric triclinic system (a = 6·69530(10) Å, b = 8·67300(10) Å, c = 9·98270(10) Å, a = 72·0270(10)°, b = 71·1900(10)°, g = 67·7830(10)°). The *g*-form crystallizes in a monoclinic cell ($C2/c$, a = 16·9695(2) Å, b = 5·46140(10) Å, c = 23·0688(3) Å, b = 110·8560(10)°).

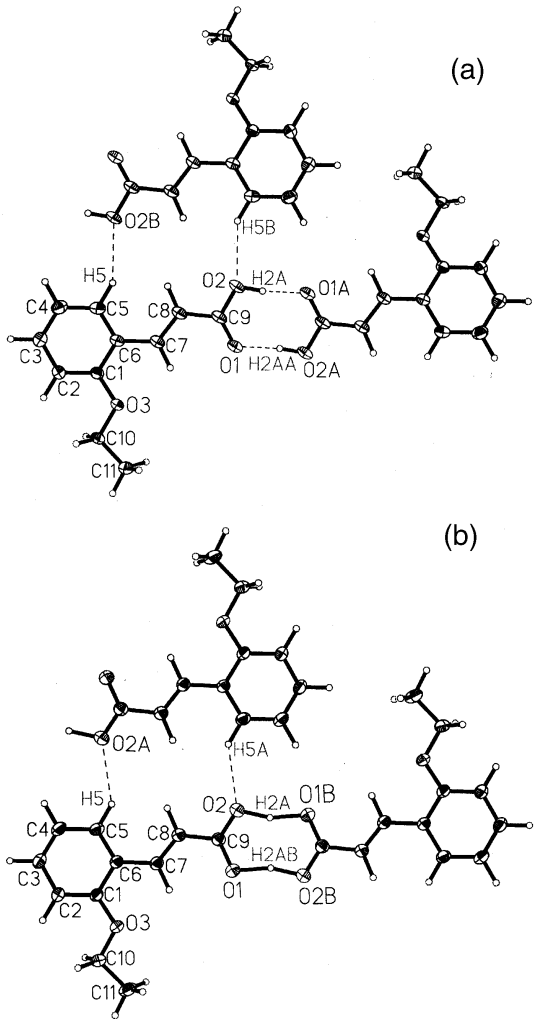

Figure 1. Packing diagrams of *o*-ethoxy cinnamic acid molecules in the (**a**) *a*- and (**b**) *g*-forms. Intermolecular contacts are also shown. All non-hydrogen atoms are shown at 50% probability ellipsoids.

Table 2. Important differences in the molecular structure in the *a*- and *g*-forms and the *a*-dimer.

	a	*g*	*a*-dimer
(a) Bond lengths (Å)			
C(6)–C(7)	1·461(2)	1·462(2)	1·509(4)
C(7)–C(8)	1·345(2)	1·335(2)	1·549(4)
C(7)–C(8A)[a]			1·580(4)
C(8)–C(9)	1·468(2)	1·468(2)	1·497(4)
O(1)–C(9)	1·240(2)	1·2710(14)	1·239(4)
O(2)–C(9)	1·3161(14)	1·278(2)	1·307(4)
O(2)–H(2A)	0·96	1·25	0·96
C(1)–O(3)	1·3648(14)	1·3675(13)	1·373(4)
O(3)–C(10)	1·4371(13)	1·431(2)	1·436(4)
C(10)–C(11)	1·506(2)	1·514(2)	1·507(6)
(b) Bond angles (°)			
C(5)–C(6)–C(7)	122·20(10)	122·74(10)	119·7(2)
C(6)–C(7)–C(8)	125·43(12)	125·78(10)	118·9(2)
C(7)–C(8)–C(9)	121·06(12)	121·87(10)	115·1(2)
C(1)–C(6)–C(7)	119·57(10)	119·18(9)	122·4(2)
O(2)–C(9)–C(8)	113·61(11)	116·56(10)	114·7(2)
O(1)–C(9)–C(8)	123·5(2)	120·49(10)	121·9(3)
O(3)–C(1)–C(6)	116·23(10)	115·88(9)	114·3(3)
C(1)–O(3)–C(10)	117·79(9)	118·03(9)	118·3(2)
O(3)–C(10)–C(11)	107·35(10)	106·97(11)	107·0(3)
(c) Torsion angles (°)			
C(5)–C(6)–C(7)–C(8)	1·6(2)	5·05(18)	–125·8(3)
C(2)–C(1)–C(6)–C(7)	–178·68(12)	–179·28(10)	176·5(3)
C(1)–C(6)–C(7)–C(8)	–179·56(12)	–175·68(11)	54·4(4)
C(6)–C(7)–C(8)–C(9)	–178·34(12)	177·94(10)	109·9(3)
C(7)–C(8)–C(9)–O(2)	–177·01(12)	175·33(11)	160·4(2)
C(7)–C(8)–C(9)–O(1)	3·7(2)	–5·60(18)	–22·6(4)
C(1)–O(3)–C(10)–C(11)	–178·87(11)	174·06(11)	–174·7(3)
C(10)–O(3)–C(1)–C(6)	–177·98(11)	–173·18(11)	–179·0(3)
C(10)–O(3)–C(1)–C(2)	1·67(18)	7·07(17)	2·7(5)

[a]The distances between the shortest double bond contact in *a*- and *g*-form are 4·514 and 5·253 Å respectively

In both these polymorphs, the asymmetric unit comprises a full molecule. We show the molecular packing diagrams of the *a*- and *g*-forms in figure 1. The structural parameters of the two forms are listed in table 2 along with those of the photodimer, to highlight the differences. We notice that the bond distances and angles in the phenyl ring as well as the double bond regions are similar, while the ethoxy groups of the two forms exhibit small differences. The torsion angles of the ethoxy and the double bond group regions are, however, noticeably different in the two forms. The molecule is non-planar in the *g*-form, the groups being twisted away from the plane of the benzene ring by as much as 9°. In the *a*-form, the heavy atom framework of the molecule is essentially planar, the side groups being out of plane of the benzene ring by ~ 3°.

In table 3, we list favourable hydrogen contacts in the *a*- and *g*-structures. There are intermolecular O–H···O contacts between the carboxyl groups in both the forms, but the nature of these contacts is entirely different. Thus, C(9)–O bond lengths in the *a*-form are 1·240(2) and 1·3161(14) Å respectively, while these distances are nearly equal (~ 1·275 Å) in the *g*-form. The intermolecular O···O distance in the *a*-form is slightly longer than in the *g*-form (*a*, 2·633(1); *g*, 2·617(2) Å). C(8)–C(9)–O(1) and C(8)–C(9)–O(2) bond angles show the some differences as well. The angles are 123·5(2)° and 113·61(11)° respectively in the *a*-form and are closer in the *g*-form, 120·49(10)° and 116·56(10)° respectively. These structural features suggest the presence of a near-symmetric hydrogen bond in the carboxylic dimer in the *g*-form and normal dimer hydrogen bond in the *a*-form. The two carboxylic bond angles approaching a common value and the bonds becoming nearly equal is in accordance with the VSEPR model. In order to explore how common such a feature is, a search was carried out using the Cambridge Structural Database (version 5.7) for carboxylic acids having the two C–O bonds differing within 0·01 Å. Of the total of 3334 acid groups found, only 3% could satisfy this criterion. Among half of these, HFIX had been applied for positioning hydroxyl hydrogen. Where hydrogen has been located, the O–H bond length ranges between 1·0 and 1·31 Å. Accordingly, the carboxylic hydrogen, H(2A) in the *g*-form was located midway in the intermolecular region with O–H and H···O distances being 1·25 and 1·40 Å respectively. This hydrogen was held at this position in the subsequent refinements. The corresponding distances in the *a*-form are 0·96 and 1·68 Å respectively (see tables 2 and 3).

Table 3. Intra- and intermolecular hydrogen bond contacts.

Polymorph	D–H…A	Bond type	H…A	D···A	∠D–H…A
a-form	O(2)–H(2A)···O(1)[a]	Acid dimer	1·68(2)	2·633(1)	172·1(6)
	C(5)–H(5)···O(2)[b]	Intralayer	2·437(1)	3·404(2)	148·9(1)
	C(4)–H(4)···O(1)[c]	Interlayer	2·637(1)	3·634(2)	153·9(1)
	C(10)–H(10A)···O(3)[d]	Interlayer	2·930(2)	3·616(2)	122·9(1)
	C(10)–H(10B)···O(1)[e]	Interlayer	2·600(1)	3·315(1)	124·3(1)
	C(11)–H(11C)···O(2)[f]	Interlayer	2·675(2)	3·648(2)	152·4(1)
g-form	O(2)–H(2A)···O(1)[g]	Acid dimer	1·40(1)	2·617(2)	162·4(8)
	C(5)–H(5)···O(2)[f]	Intralayer	2·481(1)	3·386(1)	141·2(1)
	C(4)–H(4)···O(1)[i]	Interlayer	2·615(1)	3·641(1)	159·4(1)
	C(10)–H(10B)···O(3)[j]	Interlayer	2·818(1)	3·690(1)	139·6(1)
	C(11)–H(11B)···O(1)[k]	Interlayer	2·939(1)	3·714(1)	130·3(1)
a-dimer	O(2)–H(2A)···O(1)[l]	Acid dimer	1·67(2)	2·627(3)	174(5)
	C(7)–H(7)···O(3)[m]	Intramolecular	2·42(4)	2·938(4)	108(2)
	C(8)–H(8)···O(3)[n]	Intramolecular	2·75(4)	3·176(3)	103(2)
	C(11)–H(11B)···O(1)[m]	Intramolecular	2·67(5)	3·525(5)	137(4)
	C(4)–H(4)···O(2)[p]	Intermolecular	2·60(3)	3·493(4)	140(3)
	C(11)–H(11A)···O(1)[q]	Intermolecular	2·55(5)	3·490(4)	148(3)

Symmetry: (a) $-1-x, 2-y, -z$; (b) $-1-x, 3-y, -z$; (c) $x, 1+y, z$; (d) $-x, 2-y, 1-z$; (e) $1+x, y, z$; (f) $-x, 2-y, -z$; (g) $\frac{1}{2}-x, 5/2+y, \frac{1}{2}-z$; (i) $-\frac{1}{2}-x, -\frac{1}{2}+y, z$; (j) $\frac{1}{2}-x, -\frac{1}{2}+y, \frac{1}{2}-y$; (k) $x, y-1, z$; (l) $-1-x, -y, z$; (m) $-x, -y, -z$; (n) x, y, z; (p) $x, \frac{1}{2}-y, -\frac{1}{2}+z$; (q) $x, \frac{1}{2}-y, \frac{1}{2}-z$

As shown in figure 1, each molecule is held by two C–H···O contacts from an adjacent molecule related by inversion. In the *a*-form, this contact is at 2·437(1) Å, almost perpendicular to the O–H···O contacts. The contact in the *g*-form is longer by ~ 0·05 Å and is slightly tilted following reorientation of the carboxylic group. The molecules pack in layers in both the forms, the spacing between the layers being ~ 3·45 and 3·39 Å respectively in the *a*- and the *g*-forms. The relative positions of the benzene rings in a layer do not differ appreciably in the two polymorphs and the crystal densities are also comparable (see table 1). The layers are held by C–H···O contacts, four in the α-form and three in *g*-form, the distances ranging between 2·60 and 2·94 Å (see table 3). The adjacent layers are less displaced with respect to one another in the *a*-form, with more favourable contacts in terms of the distance and the angle. The differences in the structural features of the *a*- and the *g*-forms discussed hitherto play an important role in determining the photoreactivity. We shall discuss this aspect along with the charge density, later in the paper.

We felt that the difference between the *a*- and the *g*-forms with respect to the nature of hydrogen bonding in the carboxylic acid dimer needs further proof by an independent method. Since infrared (IR) spectroscopy is ideally suited to distinguish symmetric and asymmetric hydrogen bonds [19,20], we carried out a comparative study of the IR spectra of the *a*- and the *g*-forms in the 4000–400 cm^{-1} region. The spectra were recorded in the form of KBr pellets as well as nujol mulls. The nujol mull spectra were considered essential in order to avoid spurious bands due to any moisture in KBr. In figure 2, we show the IR spectra of the two forms in the 3300–2200 and 1900–1500 cm^{-1} regions. While the spectrum of the *g*-form shows a larger number of features due to the lower symmetry as expected, the most prominent difference in the spectra of the two forms is seen in the 3300–2200 cm^{-1} region. The *a*-form shows a broad intense band centred around 3000 cm^{-1}, in addition to weak features between 2800 and 2500 cm^{-1}. Such features are characteristic of carboxylic acid dimmers [19,21]. The intense band centred around 3000 cm^{-1} is completely absent in the spectrum of the *g*-form. One of the characteristic features of symmetric hydrogen bonds is the absence of 3000 cm^{-1} band in the hydrogen bond region [20,22]. The *a*-form shows bands at ~ 1730 and 1694 cm^{-1} due to the OH bending and the C=O stretching modes respectively. We observe the C=O stretching mode at ~ 1688 cm^{-1} in the spectrum of the *g*-form, the lower C=O frequency being consistent with the stronger hydrogen bonds present in the dimer. The absence of the OH bending frequency suggests that the hydrogen bond in the *g*-form is different from that in the ordinary cyclic dimers. A symmetric H-bond does not exhibit such a bending vibration frequency. Furthermore, the appearance of additional bands at 1622 and 1598 cm^{-1} in the spectrum of the *g*-form also supports this observation [20,22]. The IR spectrum of maleate ion shows the O–H stretching band below 1650 cm^{-1}. Based on the IR studies, we can safely conclude that the *g*-form has symmetric hydrogen bonds while the *a*-form possesses the usual carboxylic acid dimers.

The photodimer of the *a*-polymorph, 2,2′-diethoxy *a*-truxillic acid, crystallizes in a centrosymmetric space group, $P2_1/c$ (a = 8·333(4) Å, b = 8·444(2) Å, c = 13·975(4) Å, b = 106·64(3)°) with two molecules per unit cell, the asymmetric unit being half the molecule. The C(7)–C(8) distance in the cyclobutyl ring is 1·549(4) Å, about 0·2 Å longer compared to the pristine *a*-form. The internal

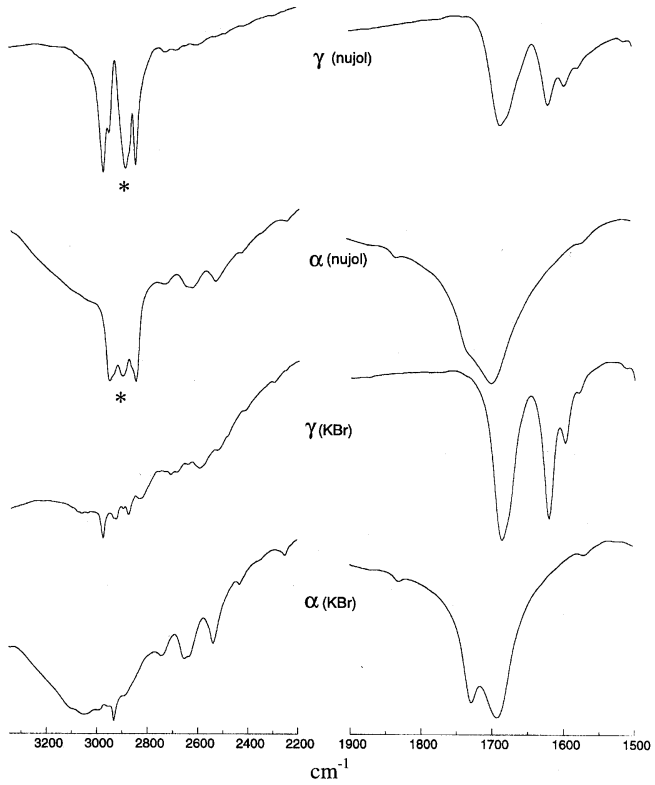

Figure 2. Infrared spectra of the *a*- and the *g*-forms of *o*-ethoxy cinnamic acid in KBr pellet and nujol mull. Asterisks denote nujol bands.

geometry of this ring is quite comparable to that found in *a*-truxilic acid [2]. The bond angles change dramatically, the angles around C(7) and C(8) become nearly tetrahedral on dimerization (see table 2). The C(6)–C(7) and C(8)–C(9) distances increase by ~0·04 Å and 0·03 Å respectively. The bond distances increase by ~0·01 Å in the ethoxy groups. The regions of the benzene ring exhibit minor changes on dimerization, but the angular relations with the side groups undergo major changes. Thus, the cyclobutyl ring and the acid groups subtend angles of ~89·4° and 46·3° respectively with the phenyl ring, while the ethoxy group makes an angle of 5·4° with the phenyl ring (compared to 2·6° in the *a*-form). In figure 3, we show the packing diagram of the photodimer viewed along the *b*-axis. The O–H···O contacts of the acid dimeric units run parallel to the *a*-axis, providing enough scope for several C–H···O side interactions (table 3). The methyl hydrogen, H(11A) establishes an intermolecular contact with a carbonyl oxygen while H(11B) forms an intramolecular contact with it. The phenyl hydrogen, H(4) enters into intermolecular contact with a neighbouring hydroxyl oxygen, O(2). Unlike the monomers, H(5) in the dimer is no longer in a position to form a C–H···O contact.

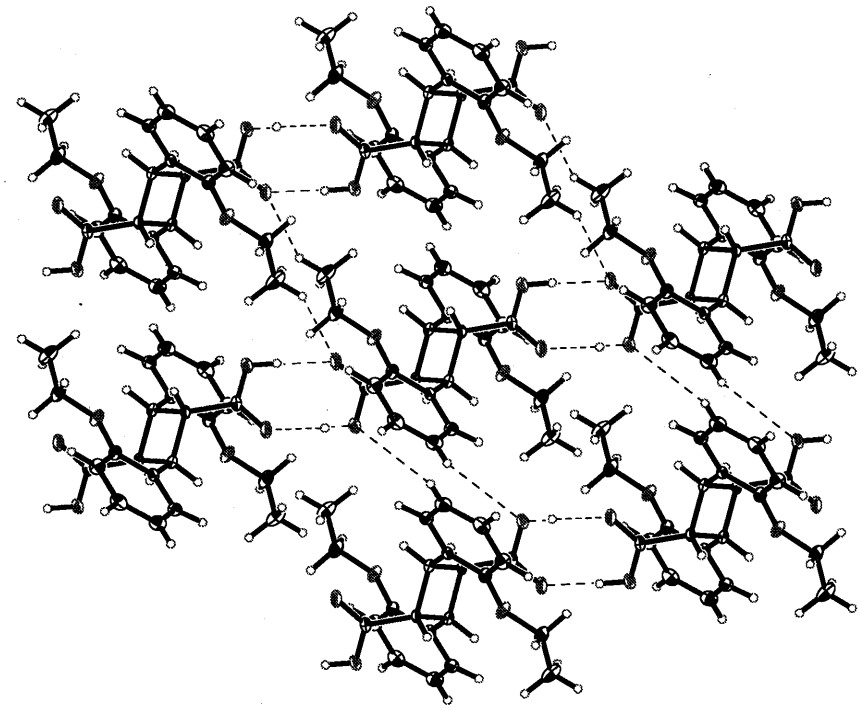

Figure 3. Packing diagram of the photodimer, 2,2′-diethoxy *a*-truxillic acid. Intra- and intermolecular contacts are also shown. All non-hydrogen atoms are shown at 50% probability ellipsoids.

In figure 4 we show two centrosymmetric molecules in the *a*-form undergoing photodimerization. The molecules belong to adjacent layers and are related by ($-x$, $2-y$, $-z$). The double bonds (1·345(2) Å) between C(7) and C(8) of the cinnamoyl groups may be considered the opposite sides of an imaginary rectangle distorted by ~ 3·1°. Although the distance between the double bonds (4·514 Å) is somewhat larger than required by the Schmidt criterion [1], the bonds are potentially reactive. In the photostable *g*-form, however, the C(7)=C(8) bond sticks out of the molecular plane (C(1)–C(6)–C(7)–C(8), –175·68(11)°, C(5)–C(6)–C(7)–C(8), 5·05(18)° as compared to –179·56(12)° and 1·6(2)° in the *a*-form) and as a result its reactive partner ($\frac{1}{2}-x$, $\frac{3}{2}-y$, $-z$) is placed farther apart (~ 5·251 Å) in an oblique parallelogram (see inset of figure 4), the acute angle being 80·7°. The cyclobutane ring formed by the dimerization of the *a*-form is not an exact square (1·549 Å × 1·580 Å), the new C(7)–C(8A) and C(8)–C(7A) bonds are slightly longer than the C(7)–C(8) bonds and the angular distortion is 1·8°. Probably, the eclipsing interactions between C(6) of the phenyl ring and C(9A) of the carboxylic group bring about subtle differences in bond lengths between the two pairs. The two halves of the dimer are related by inversion as expected from the topochemistry of the dimerization.

We now turn to the charge density analysis of the cinnamic acid monomers in the *a*- and the *g*-forms and of the photodimer. In figure 5, we show the deformation density in a plane containing C(4), C(9) and C(11) atoms of the *a*- and *g*-

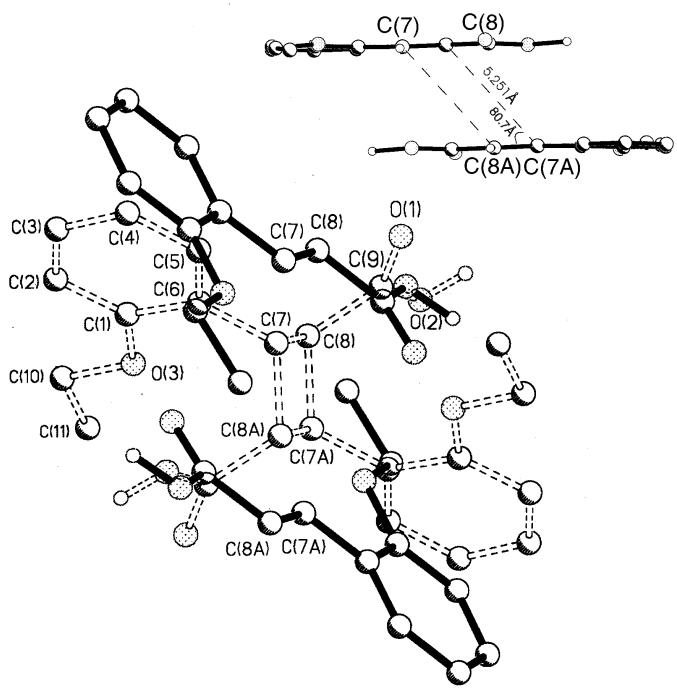

Figure 4. Photodimerization in *o*-ethoxy cinnamic acid. Two centrosymmetric molecules of the *a*-form before (full lines) and after (dashed lines) the reaction. Hydrogen atoms other than the hydroxylic are omitted from the figure for the sake of clarity. The inset shows an equivalent region containing two centrosymmetric molecules of the *g*-form.

polymorphs. Concentric contours typify the various bonding regions in the molecules between the atom-cores. The lone-pair electrons on the ethoxy and carboxylic oxygens are clearly seen as pairs of lobes. The total electron densities and the Laplacians at the critical points are listed for the various bonds in table 4 along with the polarization and ellipticity parameters. The average r_{CP} of the phenyl ring is 2·11 eÅ^{-3} in the *a*-form as compared to 2·19 eÅ^{-3} in the *g*-form. Similarly, the C(6)–C(7) and C(8)–C(9) single bond regions in the *a*-form have densities of 1·78(4) and 1·82(5) eÅ^{-3} respectively while those in the *g*-form exhibit somewhat higher values, 1·96(4) and 1·95(5) eÅ^{-3} respectively. In the *g*-form, the topography of the deformation density in the C(7)=C(8) region is as expected of a carbon-carbon double bond [23]. In the *a*-form, on the other hand, the contours are less dense (see figure 5). This is reflected in the properties of the bond CPs. In the *g*-form, the density between C(7) and C(8) is 2·55(5) eÅ^{-3}, typical of an isolated double bond [15] while in the *a*-form, it is considerably lower (2·27(5) eÅ^{-3}) though the corresponding bond lengths hardly differ (table 2). The bond in the *a*-form is associated with slightly higher ellipticity. The ethoxy groups in the *a*- and *g*-forms also show differences in bond densities. The C(1)–O(3) bond in the *a*-form has much higher density (2·21(5) eÅ^{-3}) than the O(3)–C(10) bond (1·80(5) eÅ^{-3}),

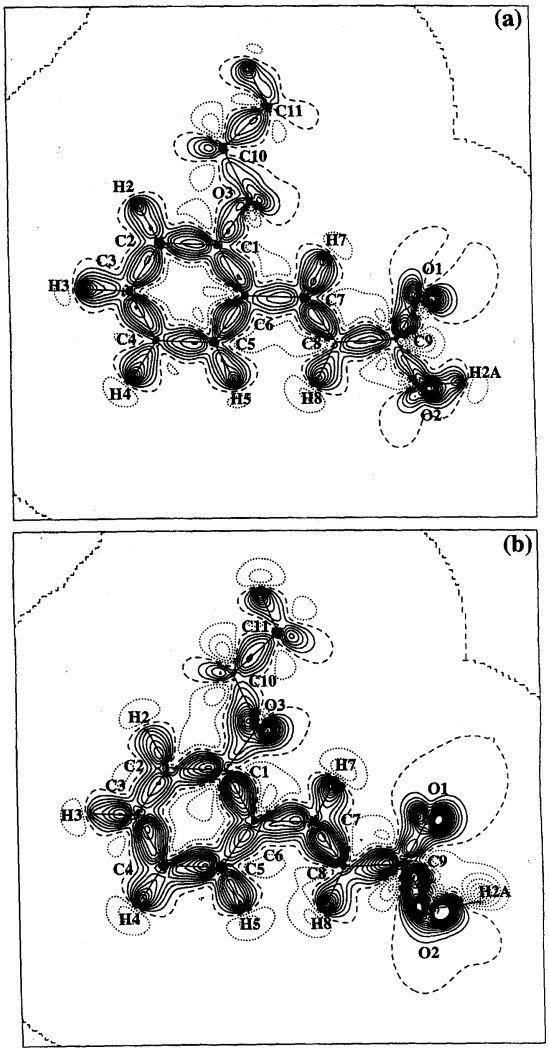

Figure 5. Deformation density maps in the mean plane of the molecule in the (**a**) *a*- and (**b**) *g*-forms. Deformation density was obtained as the difference between the total density and the spherical density without thermal smearing. Contour interval = 0·1 eÅ^{-3}.

indicating that the density has migrated from one bond to the other. The difference is much smaller in the *g*-form (~ 0·2 eÅ^{-3}). Considering that the molecule is quite planar in the *a*-form we would expect such differences due to conjugation [24].

As regards the C–H···O hydrogen contacts, all except C(10)–H(10B)···O(1) are associated with small densities and Laplacians in both the polymorphs. The C(10)–H(10B)···O(1) contact exists only in the *a*-form and carries a density of 0·052(7) eÅ^{-3} and a positive Laplacian (0·759(4) eÅ^{-5}) as expected. Following Mallinson *et*

Table 4. Analysis of bond critical points.

	a				*g*				*a*-dimer			
Bond	r	$\nabla^2 r$	e	Δ(%)	r	$\nabla^2 r$	e	Δ(%)	r	$\nabla^2 r$	e	Δ(%)
O(1)–C(9)	2·90(7)	–38·9(4)	0·38	22	2·71(7)	–38·1(4)	0·21	25	3·55(9)	–66·4(5)	0·24	23
O(2)–C(9)	2·22(7)	–26·0(3)	0·41	25	3·21(6)	–41·3(3)	0·27	15	2·83(9)	–34·4(6)	0·11	36
O(2)–H(2A)	2·3(1)	–23·8(8)	0·01	54	0·9(1)	–2·8(5)	0·1	53	2·6(2)	–39(1)	0·06	51
C(1)–C(2)	2·12(5)	–18·9(1)	0·25	2	2·22(5)	–20·9(1)	0·31	3	2·56(6)	–28·6(2)	0·32	1
C(1)–C(6)	2·02(5)	–15·9(1)	0·36	1	2·28(5)	–22·9(1)	0·35	12	2·51(7)	–31·5(3)	0·24	16
C(2)–C(3)	2·09(5)	–17·6(1)	0·26	1	2·05(5)	–15·6(1)	0·34	3	2·33(7)	–22·7(3)	0·12	13
C(3)–C(4)	2·11(5)	–17·1(2)	0·3	4	2·30(5)	–19·6(2)	0·3	5	2·29(7)	–26·3(2)	0·3	10
C(4)–C(5)	2·04(5)	–16·9(2)	0·29	5	2·27(5)	–17·9(1)	0·3	8	2·27(6)	–22·9(2)	0·1	13
C(5)–C(6)	2·14(5)	–19·9(1)	0·3	3	2·00(5)	–16·5(1)	0·28	7	2·21(9)	–22·0(5)	0·87	34
C(2)–H(2)	1·7(1)	–12·9(3)	0·15	34	1·9(1)	–20·1(4)	0·08	39	1·9(1)	–19·9(5)	0·1	38
C(3)–H(3)	1·8(1)	–15·5(2)	0·06	29	1·8(1)	–18·9(4)	0·07	42	1·9(1)	–17·1(3)	0·06	28
C(4)–H(4)	1·8(1)	–16·9(3)	0·07	28	1·9(1)	–16·9(3)	0·03	27	2·1(1)	–32·2(6)	0·09	47
C(5)–H(5)	1·8(1)	–15·6(3)	0·15	32	2·0(1)	–21·7(4)	0·1	35	1·9(1)	–19·4(3)	0·07	24
C(6)–C(7)	1·78(4)	–12·3(1)	0·23	3	1·96(4)	–14·2(1)	0·21	3	1·82(5)	–17·8(1)	0·11	1
C(7)–C(8)	2·27(5)	–21·9(2)	0·42	3	2·55(5)	–24·3(2)	0·25	5	1·63(5)	–11·7(1)	0·13	8
C(7)–C(8A)									1·54(8)	–10·6(2)	0·19	1
C(7)–H(7)	1·9(1)	–19·1(3)	0·09	37	1·84(8)	–16·3(2)	0·09	20	1·8(1)	–19·4(4)	0·07	38
C(8)–C(9)	1·82(5)	–14·0(1)	0·3	1	1·95(5)	–17·8(2)	0·26	14	2·10(6)	–25·8(2)	0·22	18
C(8)–H(8)	1·8(1)	–17·4(3)	0·11	27	1·74(8)	–14·1(2)	0·14	22	1·8(1)	–17·6(3)	0·03	34
O(3)–C(1)	2·21(5)	–16·0(2)	0·11	14	2·12(5)	–15·1(2)	0·15	17	2·28(8)	–30·9(4)	0·09	26
O(3)–C(10)	1·80(5)	–6·9(2)	0·06	13	1·91(6)	–11·6(2)	0·04	17	2·32(6)	–14·9(2)	0·08	6
C(10)–C(11)	1·71(4)	–11·1(1)	0·14	2	1·73(5)	–12·6(1)	0·17	3	1·70(7)	–12·3(2)	0·26	17
C(10)–H(10A)	1·74(7)	–11·8(2)	0·06	32	1·9(1)	–19·0(4)	0·09	36	1·8(1)	–11·1(3)	0·41	27
C(10)–H(10B)	1·82(8)	–15·0(3)	0·07	38	1·8(1)	–16·2(3)	0·11	29	1·8(1)	–13·2(4)	0·12	33
C(11)–H(11A)	1·82(8)	–12·8(3)	0·1	29	1·8(1)	–14·1(5)	0·1	40	2·1(1)	–24·4(4)	0·11	31
C(11)–H(11B)	1·6(1)	–11·1(3)	0·16	32	1·8(1)	–13·0(4)	0·13	32	1·7(1)	–11·8(5)	0·13	34
C(11)–H(11C)	1·70(8)	–10·6(2)	0·06	21	1·7(1)	–13·9(3)	0·19	25	1·8(1)	–15·2(3)	0·13	11

r in eÅ^{-3}; $\nabla^2 r$ in eÅ^{-5}

al[25], it can be considered as a moderately strong C–H···O interaction. However, the intermolecular O–H···O contacts in the two forms exhibit major differences in charge density in parallel to the structural differences discussed earlier. In this context, the deformation density maps in the carboxylic dimer region are revealing. We see from figure 5 that there are considerable differences in the charge density in this region (see tables 4 and 5). Thus, the C(9)=O(1), C(9)–O(2) and the O(2)–H(2A) regions in the *a*-form have r_{CP} values of 2·90(7), 2·22(7) and 2·3(1) eÅ^{-3} respectively. The O(2)–H(2A)···O(1A) bond carries a small density of 0·28(7) eÅ^{-3} and a positive Laplacian of 5·13(8) eÅ^{-5}, characteristic of closed-shell interaction in the intermolecular region. The near absence of distinction between the two C–O bond lengths of the carboxyl group in the *g*-form is reflected in the charge distribution. The densities associated with C(9)=O(1) and C(9)–O(2) bonds are unusually high, 2·71(7) and 3·21(6) eÅ^{-3} respectively. Moreover, we find comparable densities in the O–H and the H···O bonds (0·9(1) and 0·6(1) eÅ^{-3} respectively), the associated Laplacians being –2·8(5) and 1·9(2) eÅ^{-5} respectively. Contour maps of the Laplacian shown in figure 6 illustrate the ionic nature of the O–H bond in the *g*-form as compared to a shared interaction in the *a*-form. This is one of the few instances where the charge density distribution of a near-symmetric intermolecular hydrogen bond has been studied. In maleates containing intramolecular symmetric hydrogen bonds (O···H ~1·21 Å), the values of r_{CP} and Laplacian are ~1·1 eÅ^{-3} and –6 eÅ^{-5} respectively[5].

Inspection of the pseudo-atomic charges reveals that there is interplay between the resonance and inductive effects in the molecule. The charge on O(1), O(2) and H(2A) in the *g*-form was found to be higher (–0·47, –0·48 and 0·63 *e*) than those in

Table 5. Hydrogen bond critical points.

Polymorph	D–H…A	Bond type	r(eÅ^{-3})	$\nabla^2 r$(eÅ^{-5})
a-form	O(2)–H(2A)···O(1)[a]	Acid dimer	0·28(7)	5·13(8)
	C(5)–H(5)···O(2)[b]	Intralayer	0·04(2)	0·811(4)
	C(4)–H(4)···O(1)[c]	Interlayer	0·02(1)	0·438(5)
	C(10)–H(10A)···O(3)[d]	Interlayer	0·023(3)	0·355(2)
	C(10)–H(10B)···O(1)[e]	Interlayer	0·052(7)	0·759(4)
g-form	O(2)–H(2A)···O(1)[g]	Acid dimer	0·6(1)	1·9(2)
	C(5)–H(5)···O(2)[f]	Intralayer	0·03(1)	0·648(5)
	C(4)–H(4)···O(1)[i]	Interlayer	0·011(8)	0·300(4)
	C(10)–H(10B)···O(3)[j]	Interlayer	0·016(7)	0·319(4)
	C(11)–H(11B)···O(1)[k]	Interlayer	0·017(6)	0·277(4)
a-dimer	O(2)–H(2A)···O(1)[l]	Acid dimer	0·18(8)	5·31(8)
	C(7)–H(7)···O(3)[m]	Intramolecular	0·034(6)	0·576(4)
	C(8)–H(8)···O(3)[n]	Intramolecular	0·07(1)	1·146(5)
	C(11)–H(11B)···O(1)[m]	Intramolecular	0·05(1)	0·683(7)
	C(4)–H(4)···O(2)[p]	Intermolecular	0·02(1)	0·427(5)
	C(11)–H(11A)···O(1)[q]	Intermolecular	0·03(2)	0·622(7)

Symmetry: (a) $-1-x, 2-y, -z$; (b) $-1-x, 3-y, -z$; (c) $x, 1+y, z$; (d) $-x, 2-y, 1-z$; (e) $1+x, y, z$; (f) $-x, 2-y, -z$; (g) $\frac{1}{2}-x, \frac{5}{2}+y, \frac{1}{2}-z$; (i) $-\frac{1}{2}-x, -\frac{1}{2}+y, z$; (j) $\frac{1}{2}-x, -\frac{1}{2}+y, \frac{1}{2}-y$; (k) $x, y-1, z$; (l) $-1-x, -y, z$; (m) $-x, -y, -z$; (n) x, y, z; (p) $x, \frac{1}{2}-y, -\frac{1}{2}+z$; (q) $x, \frac{1}{2}-y, \frac{1}{2}-z$

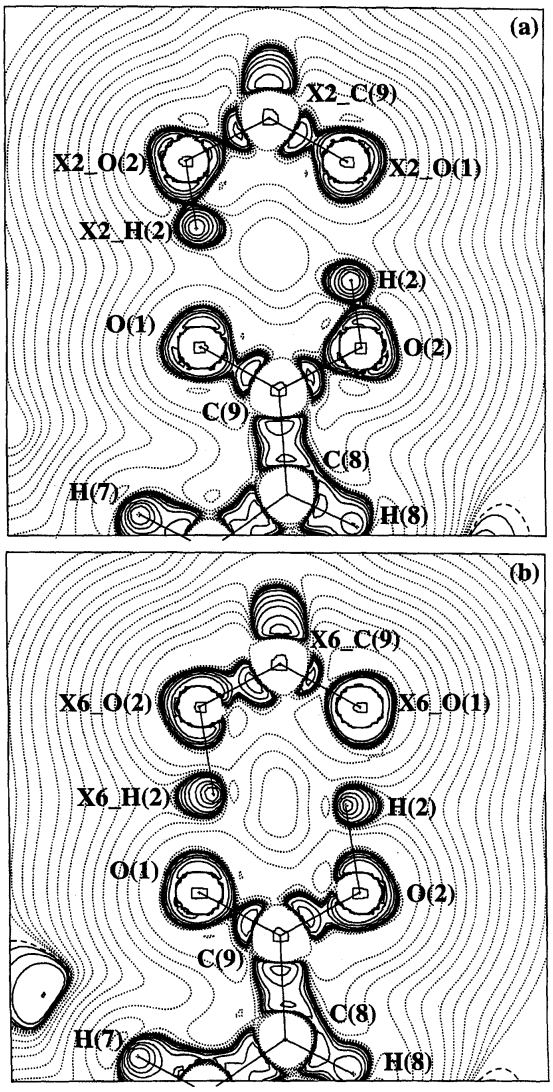

Figure 6. Contour maps of the Laplacian of the total density in the O(1), O(2) and C(9) plane for (**a**) *a*- and (**b**) *g*-forms.

the *a*-form (–0·27, –0·28 and 0·19 *e*). The ethoxy oxygen, O(3), exhibited charges of –0·39 and –0·16 in the *g*- and *a*-forms respectively. The molecular geometry in the two forms can be rationalized based on the above discussion. If the molecule in the *g* form were planar, the ethoxy group at the ortho position would pump in more charge through resonance which would simply destabilize the charge separation in the molecule. Thus, it is clear that the ionic nature of the near symmetric hydrogen bond in the *g*-form goes hand in hand with the localization of charge density in the respective bond regions and the non-planarity of the molecule.

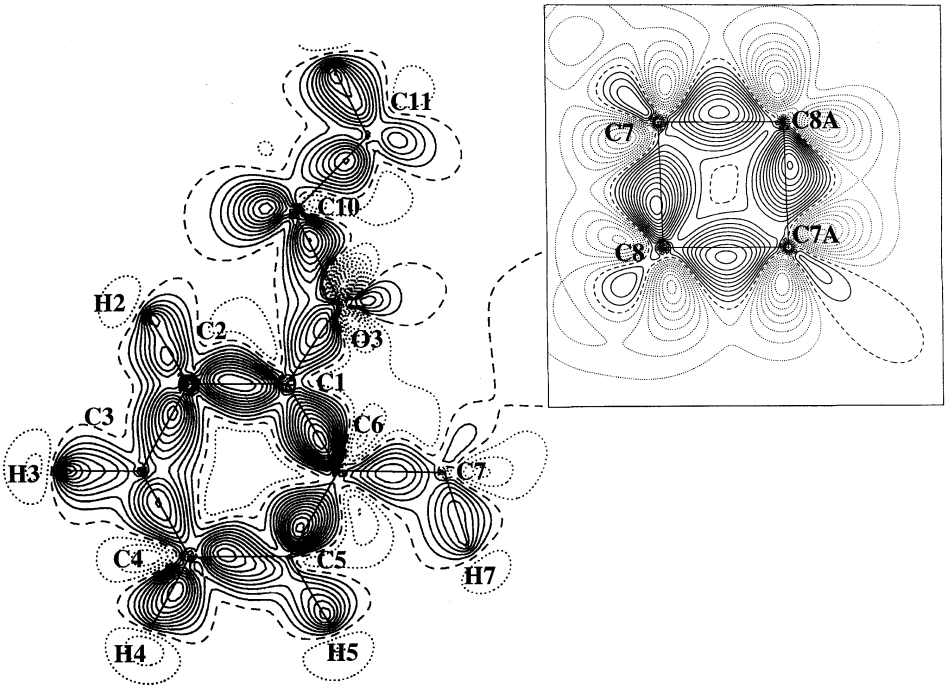

Figure 7. Deformation density map of the photodimer, 2,2′-diethoxy *a*-truxillic acid in the plane of the phenyl ring. The inset shows the deformation density in the plane of the cyclobutane ring. Contour interval = 0·075 eÅ^{-3}.

We now discuss the nature of charge distribution in the photodimer in comparison with the monomers in the two polymorphs (figure 7). The geometry and the bond properties of the dimer differ significantly not only in the reactive region but also in the other parts of the molecule. The benzene ring, however, remains essentially unaffected upon dimerization. The r_{CP} values of C(1)–O(3) and O(3)–C(10) bonds are much closer, 2·28(8) and 2·32(6) eÅ^{-3} respectively. The densities in C(6)–C(7) and C(8)–C(9) regions are typical of single bonds. The bonding within the carboxylic group resembles that in the *a*-form with r_{CP} values of 3·55(9), 2·83(9) and 2·6(2) eÅ^{-3} for C(9)=O(1), C(9)–O(2) and O(2)–H(2A) respectively. The intermolecular O(2)–H(2A)···O(1) bond carries a small density of ~ 0·18(8) eÅ^{-3} with a Laplacian of ~ 5·31(8) eÅ^{-5} as in the *a*-form. The C–H···O contacts exhibit low densities (mean value 0·04 eÅ^{-3}) and small Laplacians as listed in table 5. The cyclobutane ring resulting from the photodimerization of the *a*-form is shown in the inset of figure 7. The ring exhibits a (3, +1) CP[26] at the inversion centre with a density of ~0·62 eÅ^{-3} and a Laplacian of ~ 5·8 eÅ^{-5}. The C–C bonds of the cyclobutane ring exhibit low values of r_{CP} and Laplacians (~1·58 eÅ^{-3} and ~ –11·2 eÅ^{-5} respectively), implying that the bonds are weak. The contours in the C(7)–C(8) and C(7A)–C(8A) regions lie outside the interatomic vector. These are bent bonds characteristic of strained rings[27,28]. Ellipticity values of the C(7)–C(8) and C(7)–C(8A) bonds are high (0·13 and 0·19 respectively) compared to an ideal single

bond for which ellipticity is zero. The polarization associated with the C(7)–C(8) bond is noticeably higher (8%) compared to the value in C(7)–C(8A) ~1%.

4. Conclusions

The present study of the reactivity of *o*-ethoxy cinnamic acid has provided some fine details related to the solid state photoreactivity of this compound, involving (2+2) cycloaddition. The molecule in the reactive *a*-form is essentially planar, but in the *g*-form the side groups are out of the plane of the benzene ring. The adjacent cinnamoyl double bonds in the *a*-form face each other at a favourable distance (~4·514 Å) while in the *g*-form, the double bonds are not only placed at a larger distance (~5·251 Å) but are also not properly oriented with respect to each other. This is due to the significant differences between the structures in the two forms, the most noteworthy one being the presence of near-symmetric O–H···O hydrogen bonds in the *g*-form compared to the ordinary carboxylic dimer contacts in the *a*-form. The nature of the hydrogen bonds is confirmed by IR spectroscopy measurements. The O–H stretching frequency at ~3000 cm^{-1}, common to carboxylic acid dimers, is not observed in the spectrum of the *g*-form. Instead, two additional bands appear around 1600 cm^{-1} due to the symmetric hydrogen bond. The intermolecular C–H···O contacts in the *g*-form are considerably weakened due to the presence of the near-symmetric hydrogen-bonded dimer.

There are also important differences in the charge density distribution between two forms. The molecule being planar in the *a*-form, effects due to conjugation are clearly seen in the charge density. The r_{CP} of the double bond is considerably smaller (2·27 eÅ^{-3}) compared to that in the *g*-form (2·55 eÅ^{-3}). The ethoxy link to the phenyl ring carries some extra density due to charge migration from the ethoxy bond. Such effects are not observed in the case of the *g*-form. The symmetric hydrogen bond of the latter being ionic, the molecule prefers non-planar geometry. The cyclobutane ring formed by the dimerization is not exactly a square, the angular distortion being 1·8°. New C–C bonds are slightly longer compared to the other pair. The ring is strained, all the bonds being associated with small densities and Laplacians.

Acknowledgement

The authors thank Professor C N R Rao, FRS for suggesting the problem and for useful discussions.

References

1. Cohen M D, Schmidt G M J and Sonntag F I 1964 *J. Chem. Soc.* 2000
2. Enkelmann V, Wegner G, Novak K and Wagener K B 1993 *J. Am. Chem. Soc.* **115** 10390
3. Jeffrey G A and Piniella J F (eds) 1991 *The application of charge density research to chemistry and drug design* (New York: Plenum)
4. Ortmann I, Werner St and Kruger C 1992 *J. Am. Chem. Soc.* **114** 5048
5. Madsen D, Flensburg C and Larsen S 1998 *J. Phys. Chem.* **A102** 2177
6. Kulkarni G U, Kumardhas P and Rao C N R 1998 *Chem. Mater.* **10** 3498
7. Furniss B S, Hannaford A S, Smith P W G and Tatchell A R (eds) 1989 *Vogel's textbook of practical organic chemistry* (Harlow, Essex: Addison Wesley–Longman)

8. Siemens Analytical X-ray Instruments Inc. 1995 Madison, Wisconsin, USA
9. SHELXTL 1995 (Silicon Graphics version) Siemens Analytical X-ray Instruments Inc. Madison, Wisconsin, USA
10. Allen F H, Kennard O, Watson D G, Brammer L, Orpen A G and Taylor R 1987 *J. Chem. Soc., Perkin Trans.* II S1
11. Schomaker V and Trueblood K N 1998 *Acta Cryst.* **B54** 507
12. Hirshfeld H L 1976 *Acta Crystallogr.* **A32** 239
13. Hansen N K and Coppens P 1978 *Acta Crystallogr.* **A34** 909
14. Koritsansky T, Howard S T, Richter T, Mallinson P R, Su Z and Hansen N K 1995 XD – A computer program package for multipole refinement and analysis of charge densities from diffraction data (Cardiff, Glasgow, Buffalo, Nancy, Berlin); xd-user@chemie.fu-berlin.de
15. Cremer D and Kraka E 1984 *Croat. Chem. Acta* **57** 1259
16. Collard K and Hall G G 1977 *Int. J. Quantum Chem.* **12** 623
17. Bader R F W and Essen H 1984 *J. Chem. Phys.* **80** 1943
18. Naradelli M 1983 *Comput. Chem.* **7** 95
19. Bellamy L J 1975 *The infrared spectra of complex molecules* 3rd edn (London: Chapman and Hall)
20. Rao C N R and Ferraro J R 1970 *Spectroscopy in inorganic chemistry* (New York: Academic Press) vol. 1
21. Braunholtz J T, Hall G E, Mann F G and Sheppard N 1959 *J. Chem. Soc.* 868
22. Blinc R and Hadzi D 1960 *Spectrochem. Acta* **16** 852
23. Coppens P 1994 *Annu. Rev. Phys. Chem.* **43** 663
24. Morrison R T and Boyd R N 1989 *Organic chemistry* 5th edn (New Delhi: Prentice Hall-India)
25. Mallinson P R, Wozniak K, Smith G T and McCormack K L 1997 *J. Am. Chem. Soc.* **119** 11502
26. Bader R F W 1990 *Atoms in molecules – A quantum theory* (Oxford: Clarendon)
27. Angermund K, Claus K H, Goddard R and Kruger C 1985 *Angew. Chem., Intl. Ed. Engl.* **24** 237
28. Irngartinger H and Strack S 1998 *J. Am. Chem. Soc.* **120** 5818